Assessing focused wave applicability on a coupled aero-hydro-mooring FOWT system using CFD approach

Yang Zhou[1], Qing Xiao[1*], Christophe Peyrard[2], Guang Pan[3]

[1]Department of Naval Architecture, Ocean and Marine Engineering, University of Strathclyde, Glasgow, G4 0LZ, UK

[2]Saint-Venant Hydraulics Laboratory (Électricité de France, ENPC, Cerema), Université Paris-Est, 6 quai Watier, 78400 Chatou, France

[3]School of Marine Science and Technology, Northwestern Polytechnical University, Xi'an, 710072, PR China

*Correspondent: **qing.xiao@strath.ac.uk**

Abstract

The present study examines the wave type and wave steepness impacts onto the floating offshore wind turbine (FOWT) hydro/aerodynamics. With the aid of using a high-fidelity aero-hydro-mooring CFD solver, the current modelling focuses on the analysis of NREL 5MW semi-submersible FOWT dynamic motion response, tension load of the mooring line, wind turbine thrust, power output and tower base bending moment. Totally, three types of waves, i.e., focused wave, irregular wave and reconstructed focused wave are adopted to examine the wave type impacts on FOWT performance. Our results find that, given a same wave spectrum, a significant difference is observed for the floater motion response prediction between a focused wave and an irregular wave. However, with the use of the reconstructed focused wave, the results show very similar FOWT hydrodynamic characteristics as those obtained with the

This is a peer-reviewed, accepted author manuscript of the following article: Zhou, Y., Xiao, Q., Peyrard, C., & Pan, G. (2021). Assessing focused wave applicability on a coupled aero-hydro-mooring FOWT system using CFD approach. Ocean Engineering, 240, [109987]. https://doi.org/10.1016/j.oceaneng.2021.109987

irregular wave, indicating that the reconstructed focused wave can be an alternative of the irregular wave for extreme wave studies. Moreover, nonlinear effect is well captured for various wave steepness tested, which is revealed by the occurrence of wave diffraction and large wave run-ups near the side columns. The examination on FOWT aerodynamics found that both wave type and wave steepness have little impact on turbine aerodynamic performance which is evident by a close agreement of thrust and power prediction under different incident waves.

Keywords: Floating offshore wind turbine (FOWT), Computational Fluid Dynamics (CFD), Focused wave, wave type impacts

1. Introduction

In 2020, WindEurope report [1] showed that 2.9GW offshore wind capacity had been installed in Europe across 11 countries and covered nearly 1.5% of the annual Europe energy demand, among which most of the newly installed offshore wind farms are located in the North Sea near Norway and UK. Consequently, there is an increasing demand for the design and construction technology on the wind turbine configuration and the offshore wind substructure.

At the preliminary stage, floating offshore wind turbine (FOWT) designs usually adopt uniform wind and regular/irregular wave conditions to evaluate the hydro/aerodynamic loads and the mooring resistance. This is normally achieved by using blade element method (BEM) and potential flow theory method. They are essential but not sufficient to reach the design requirements, especially under harsh working conditions when high nonlinearity effect may occur. The Quadratic Transfer Functions (QTF) used by potential flow have limitations on predicting the nonlinear viscous force and relies on the hypothesis of small wave height and small motions. On the other hand, the fatigue damage of turbine structure and the nonlinear hydrodynamic loads are difficult to be represented by using low-fidelity analysis methods.

Therefore, it is highly worthwhile to utilise some high-fidelity approaches to study the wave-structure interaction and thus to reflect the nature of nonlinearities. The Computational Fluid Dynamics (CFD) method as one of the high-fidelity approaches, allows us to solve the fluid flow governing equations directly, and produce detailed flow variables in both the time and spatial domains so that the transient hydro/aerodynamic loading on the FOWT, can all be well resolved. Also, with the help of the improving high-performance computing capacity, the CFD method can be one of the most appropriate choices to predict FOWT nonlinear hydrodynamics under different sea states.

Generally, the wave-structure interactions under random sea state have to be studied by using physical scale models in the wave tank [2] or numerical models in the numerical wave tank (NWT), where long-duration irregular wave is commonly adopted, which is quite time-consuming and computationally expensive. However, there might be some other options to study nonlinear effect, for instance, the focused wave. The concept of focused wave was proposed by Davis et al. [3] by modulation of a series of regular wave trains generated from a prescribed wave spectrum and superimposing the crests. This was used to analyse the nonlinear wave-wave or wave-structure interaction phenomena to replace the irregular wave. Examples for sole wave-wave interaction include Baldock et al. [4], Ryu et al.[5], Orszaghova et al. [6], Liang et al. [7], and Niu et al. [8]. The usage of focused wave dramatically decreases the overall examination time with certain accuracy to predict the physical phenomena via reducing the wave reflections in the wave tank test [9], and the errorness between the prescribed and actual wave elevation [10]. Since then, the focused wave has also been adopted in several studies to investigate the wave-structure interaction and predict the extreme load on the offshore structure. Those studies are initially focused on simple floaters [11-13] and fixed structures [14-16], and then extended to complex floating structures, like FOWT or wave energy converters (WEC) [17-20]. Throughout these studies, it is evident that focused wave can represent extreme sea

state to some extent, so that the extreme load associated with the nonlinear hydrodynamics can be captured.

Although the relation between focused wave and corresponding sea state has been established, it is not clear, given a same sea state, whether using a focused wave is accurate enough to replicate the max/minimum dynamic responses of a floating structure in comparison with irregular wave. In relation to this, Zhao et al. [21] studied wave-structure interaction for a 2-D floating body under three types of wave, i.e., a regular, a focused and a combined regular and focused wave to reveal the nonlinear effects which may be induced by different waves. It was concluded that the floater performs regular responses under the regular wave while a large amplitude of roll motion and green water effect are captured under focused wave. Meulen et al. [22] investigated the impact on the fatigue loads of a fixed bottom monopile offshore wind turbine between regular wave and irregular wave. His study revealed that given the same sea state, the irregular wave overpredicts 7.5% of fatigue loads than the regular wave. His study also indicated that the wave steepness is the prominent reason to cause the above difference due to the increasing nonlinear wave load. Although these two studies covered irregular, regular, and focused wave, the initial wave energy spectrum for various wave types are entirely different, i.e., single frequency wave input for a regular wave and multiple frequency wave input for focused/irregular waves. Therefore, a direct comparison among different wave types of result is based on an inconsistent energy input.

The present study aims at presenting the first study to reveal the relation between the focused wave and irregular wave conducted on a FOWT system through an investigation of the nonlinear wave-structure interactions under a consistent wave energy input. Thus, to examine whether they can represent each other to induce similar hydrodynamic characteristics of a moored floating structure. The modelling will be achieved by using high-fidelity CFD tool

based on our previous studies [18, 23, 24]. In addition, we will extend our studies to the aerodynamic analysis of a blade resolved wind turbine under different wave types to bring fundamental insights to evaluate the wave type impact on the wind turbine structure.

2. Problem Statement

To examine the blade-resolved flow of the wind turbine in addition to the dynamic motion prediction of the floater, we use a coupled aero-hydro-mooring solver based on solving the unsteady Reynolds Average Navier Stokes (URANS) equations using a finite volume method. The details of the flow solver including the free surface modelling, numerical wave generation and absorbing, mooring li ne modelling, and mesh motion handling, details are summarised in our previous studies [18, 23, 24], therefore, only a brief introduction will be given in the following sections.

Table 1. Gross properties of OC4 Semi-Subersible NREL 5MW Wind Turbine

FOWT gross properties	
Platform mass, including ballast	14,143,400 kg
Displacement	13986.8 m^3
Platform pitch inertia about centre of mass	1.315×10^{10} kgm^2
Platform yaw inertia about centre of mass	1.906×10^{10} kgm^2
Platform roll inertia about centre of mass	1.315×10^{10} kgm^2
Water Depth	200.0 m
Surge natural period	107s
Heave natural Period	18s
Pitch natural Period	27s
Mooring Line properties	
Number of mooring lines	3
Angle between adjacent lines	120°
Radius to anchors from platform centreline	837.6 m
Mooring line diameter	0.0766 m
Equivalent mooring line mass density	113.35kg/m
Equivalent mooring line mass in water	108.63/kg/m
Equivalent mooring line extensional stiffness	753.6MN
Wind turbine properties	
Rotor configuration	3 blades
Rotor, hub diameter	126.0 m, 3.0 m
Hub height about SWL	90.0 m
Blade length	61.5 m

The FOWT model adopted in the present study is a widely used benchmark, i.e., OC4 DeepCwind semi-submersible NREL 5MW floating offshore wind turbine [25]. The semi-submersible platform consists of three large columns with heave plate bases and one central column connecting the tower and supporting the wind turbine. Three mooring lines are set around the floater with each mooring line's fairlead at each side column. The gross properties of the wind turbine, tower, floating platform is shown in Table 1 and it is referred by the NREL reports. The natural periods of FOWT for the mode of surge, pitch and heave are 107s, 18s, and 27s respectively. Due to the presence of the long natural surge oscillation periods, the time-mean position of entire floater could not reach a stationary position at the very beginning of the modelling. Therefore, for all focused wave modelling, the focused time is designed to be larger than the celerity corresponds periods (nearly 50s in the present simulations) and based on when the transient phase of the FOWT motions mitigates.

3. Numerical Methodology

3.1 Fluid flow modelling

The open-source CFD framework OpenFOAM [26] is adopted as the flow solver for the coupled aero-hydro-mooring FOWT modelling, while the flow field around the FOWT is treated as incompressible, transient and viscous. The flow field resolving is governed by the continuity and unsteady Reynolds-averaged Navier-Stokes (RANS) equations, which are written as follows,

$$\nabla \cdot U = 0 \tag{1}$$

$$\frac{\partial \rho U}{\partial t} + \nabla \cdot \left(\rho(U - U_g)U\right) = -\nabla P_t - g \cdot x\nabla\rho + \nabla\left(\mu_{eff}\nabla \mathrm{U}\right) + (\nabla \mathrm{U}) \cdot \mu_{eff} + f_\sigma \tag{2}$$

In which U and U_g is the flow velocity of the flow field and the grid nodes in Cartesian coordinates; $\nabla = \partial/\partial \mathrm{x},\ \partial/\partial \mathrm{y},\ \partial/\partial \mathrm{z}$ is the differential operator; ρ refers to the mixed density

of water and air; $\mathbf{g}$ denotes the gravity acceleration vector and $P_t = P - \rho\mathbf{g} \cdot \mathbf{x}$ is the dynamic pressure obtained by the total pressure P minus the hydrostatic pressure $\rho\mathbf{g} \cdot \mathbf{x}$. The formula $\mu_{eff} = \rho\,(v + v_t)$ is used to calculate the effective dynamic viscosity, in which v and v_t are the kinematic and eddy viscosity respectively; f_σ denotes the surface tension term.

The k-ω SST turbulence model is used in the current study to deal with a flow condition at a high Reynolds number for a typical wind turbine. This can provide a better prediction of separating flow around turbine blades and demonstrates its strength in adverse pressure gradients.

In order to deal with the free surface modelling between wave and air, the Volume of Fluid (VOF) [27] method is adopted to differentiate the two phases (water and air) by introducing the volume fraction variable α, which α equals to 0 refers to the phase of air and 1 for water, it follows the governing transport governing equation as described:

$$\frac{\partial \alpha}{\alpha t} + \nabla \cdot \mathbf{u}\alpha + \nabla \cdot [\mathbf{u_r}(1-\alpha)\alpha] = 0 \tag{3}$$

In order to capture the free surface precisely, a bounded compression method with an additional compression term is used, e.g., the last term on the left-hand side of the transport equation which only functions near free surface due to the inclusion of $(1-\alpha)\alpha$, where $\mathbf{u_r} = \mathbf{u_{water}} - \mathbf{u_{air}}$ is an artificial velocity field, and used to compress the interface.

For a two-phase flow problem, the volume fraction of each phase is used as the weighting factor to calculate the mixture properties. The equations for the density and the viscosity can be expressed as follows,

$$\rho = \alpha\rho_w + (1-\alpha)\rho_a \tag{4}$$

$$\mu = \alpha\mu_w + (1-\alpha)\mu_a \tag{5}$$

Where subscripts w and a represent water and air, respectively.

3.2 Numerical wave generation in the flow solver

The free surface water waves are generated and absorbed based on an open-source toolbox "waves2Foam" [28] in a numerical wave tank (NWT) , while the relaxation zone technique is adopted to provide better wave quality near the inlet boundary and avoid wave reflection near the outlet boundary. In the present work, a widely accepted design-wave in offshore engineering known as "NewWave" is used to reproduce extreme events [29] [30]. Two wave types are adopted in this study, i.e., focused wave and irregular wave. The focused wave, based on the linear NewWave theory, is generated via the linear superposition of a series of regular waves. The wave amplitude and wave frequency of each wave component is determined according to the discretization of a prescribed wave spectrum, the wave components, and the linear crest amplitude. The phase of each wave component is adjusted to reach the maximum wave elevation at the prescribed focused time and position. The linear NewWave theory is also adopted to generate the irregular wave in the NWT without modulating the phase of each wave component. Detailed explanation is given in the following equations.

The JONSWAP spectrum is selected as the input surface spectral density, which is given as,

$$\mathrm{S}(f) = 0.204 H_s^2 f_p^4 f^{-5} (-\frac{5}{4}) \exp((\frac{f}{f_p})^{-4}) \gamma^r \tag{6}$$

$$r = \exp[\frac{-(f - f_p)^2}{2\sigma^2} {f_p}^2] \tag{7}$$

While *Hs* represents the significant wave height, f_p denotes the peak frequency, and the peak enhanced factor γ equals to 3.3 for all simulations. The peak shape factor σ is defined as,

$$\sigma = \begin{cases} 0.09 & f \geq f_p \\ 0.07 & f < f_p \end{cases} \tag{8}$$

The incident wave spectrum is then discretised into a given number of discrete frequencies, while each of them represents a single regular wave component, and the linear superposition of all wave trains forms the NewWave. The surface elevation can be represented into the time domain by the linear formation,

$$\eta(x,t) = \sum_{i=1}^{N} a_i * \cos(k_i x - 2\pi f_i t + \varphi_i) \tag{9}$$

a_i , k_i , f_i denotes the wave amplitude, wave numbers and wave frequencies of the regular wave components, respectively. φ_i is the phase lag in the interval [0, 2π]. a_i is calculated based on the given wave spectrum and linear crest amplitude A_0,

$$a_i = A_0 * \frac{0.5 * [S(f_{i-1}) + S(f_i)]\Delta f_{i-1}}{\int_{i=1}^{N} 0.5 * [S(f_{i-1}) + S(f_i)]\Delta f_{i-1}} \tag{10}$$

$\Delta f_{i-1} = f_i - f_{i-1}$ is considered as equidistant discretization which determined by the number of the wave components *N* and the bandwidth, given as,

$$\Delta f_i = \frac{f_u - f_l}{N - 1} \tag{11}$$

f_u and f_l represents the maximum and minimum limit of frequency bandwidth, and those are chosen as $4f_p$ and $0.3f_p$, respectively, to guarantee most of the wave energy range is covered. The bandwidth *N* is selected as 200 as it is found that the wave components do not significantly affect the wave surface elevation near the focused position and time, pointed out by Jacobsen [31] and Hu's study [32]. The periodicity repetition of the NewWave refers to $T' = 1/\Delta f_i$ =810s. For all focused wave cases, the time window for wave generation is set as 300s,

which is short enough to have repetition. However, for irregular wave simulation, it is practically very computationally expensive to simulate a coupled FOWT using high-fidelity CFD at a time frame of 3 hours. For the current work, the time window is selected as the repetition period of the waves, i.e., $T' = 810s = 54Tp$ for LC*.2 (referred Table 2).

In order to achieve a large amount of wave trains energy at a fixed time spot, the modulation of phase angle among individual wave components is conducted to generate focused wave. The random phases of each wave component have to satisfy the following equation,

$$\cos\left(k_i x - 2\pi f_i \mathrm{t} + \varphi_i\right) = 1 \tag{12}$$

The phase angle of the wave component can then be written as,

$$\varphi_i = k_i x - 2\pi f_i \mathrm{t} - 2\pi n, n = 0,1,2, \ldots \tag{13}$$

The vertical and horizontal velocities w and u implemented to the inlet boundary are given by,

$$w(x,t) = \sum_{i=1}^{N} \frac{a_i g k_i}{2\pi f_i} \frac{\sinh k_i(z+h)}{\cosh(k_i h)} \sin(k_i(x - x_0) - 2\pi f_i(\mathrm{t} - t_0) \tag{14}$$

$$u(x,t) = \sum_{i=1}^{N} \frac{a_i g k_i}{2\pi f_i} \frac{\cosh k_i(z+h)}{\cosh(k_i h)} \cos(k_i(x - x_0) - 2\pi f_i(\mathrm{t} - t_0) \tag{15}$$

g is the gravitational acceleration, while z refers to the vertical length measured upwards from the still water level, h is the water depth. x_0 and t_0 representing the focused position and focused time, respectively.

3.3 Mooring Line modelling

In order to predict the tension loads of the mooring lines, a static mooring line modelling module is implemented in our CFD tool [33]. Specifically, the mooring line is not directly modelled in the CFD computational domain. Instead, the tension loads of the mooring are

added as constraints on the patches of the floater onto the computational mesh. The mooring lines are divided into a given number of segments. In the present simulations, each line is devided into 40 segments to capture the tension load accurately. The loads on each segment are solved with the force equilibrium equations along with horizontal and vertical directions by considering the hydrodynamic forces, the line weight together with the tension loads, the hydrodynamic forces are also care calculated by using Morison's equation [34] which considered both the drag loads and inertia force. For the drag force, it is estimated by the flow velocity, segment velocity and a prescribed drag coefficients both in tangential and normal directions in the local reference frame. Similarly, the inertia force is calculated by the relative flow acceleration and the added mass coefficients in both directions in the local reference frame.

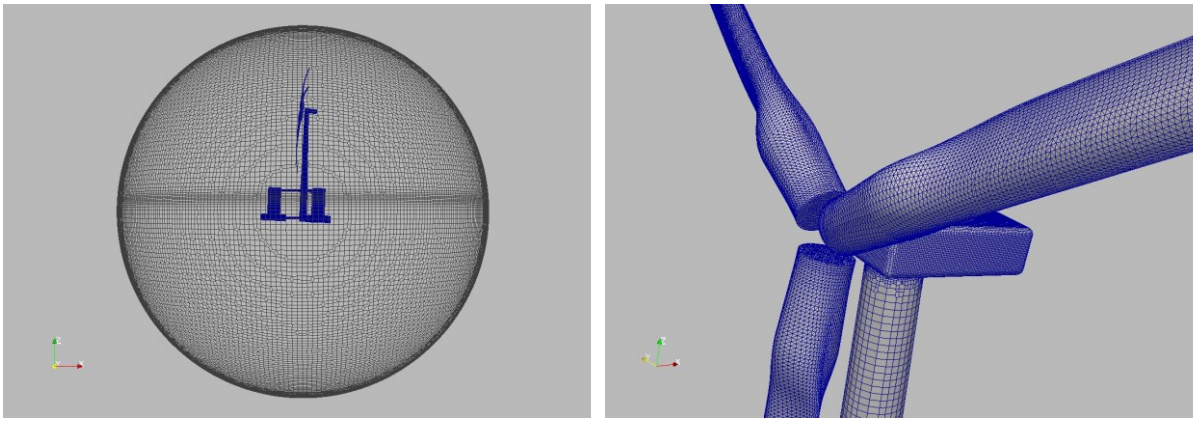

Figure 1 Computational mesh of NREL 5MW semi-submersible FOWT

3.4 Numerical methods

The PIMPLE algorithm (a combination of PISO: Pressure Implicit with Splitting of Operators and SIMPLE: Semi-Implicit Method for pressure-linked Equations) is utilised to solve the pressure-velocity coupling. The maximum allowed Courant number can be set as large as 50, and the time step is fixed as small as 0.002s (around 1/7000Tp, Tp refers to the incident wave peak period). The computational cost is nearly 120 hours and 320 hours for a typical case of 300 seconds focused wave and 810 seconds irregular wave, respectively. This is obtained using High Performance Computing facility with 360 cores running in parallel. Figure 1 shows the

mesh around the blades and tower and the sliding mesh surface of the computational domain. A built-in mesh generation tool in OpenFOAM is adopted to generate the computational mesh. The total mesh for the present CFD computation is around 6,844,520. The floater is allowed to rotate and translate freely in the surge, pitch and heave directions while a built-in arbitrary mesh interface (AMI) method in OpenFOAM is used to analyse the motion of floating wind turbine.

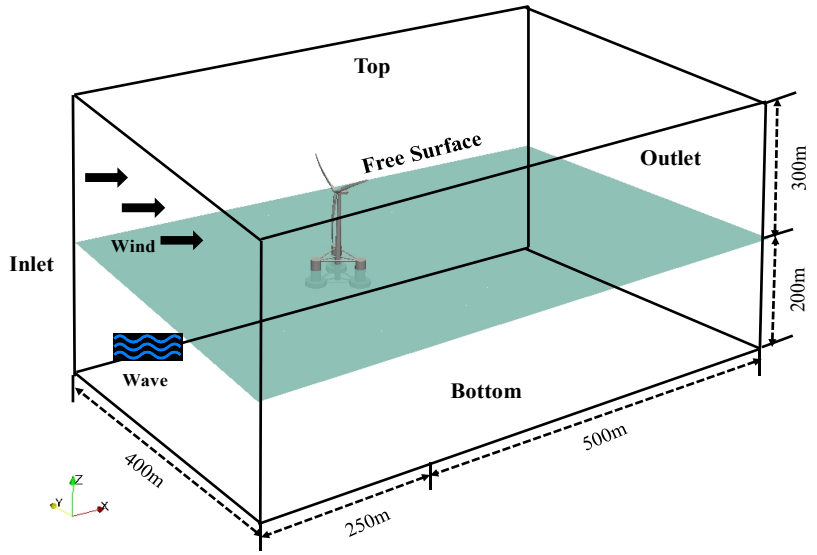

Figure 2 Sketch of computational domain

Figure 2 plots the sketch of the boundary conditions of the CFD domain. At the inlet boundary (where $x = -250m$), the velocity is defined as the prescribed incident irregular/focused wave together with uniform wind field in the air. The front and back boundaries ($y = \pm 200m$) are imposed as symmetric boundaries and the top and bottom boundaries ($z = 300m$ and $-200m$) are set as the zero gradient. The non-slip wall boundary with zero pressure gradient is defined on all the patches of the FOWT. The upstream region (250m) and the downstream region (500m) is nearly 1.6λ and 3.3λ for LC1.1, where λ refers to the wavelength of the incident wave. The inlet and outlet relaxation zone used to guarantee the accuracy of the incident wave and reduce the reflection waves [32] extends to 1λ and 2.3λ, respectively.

4. Selected case studies

In order to investigate the FOWT hydro/aerodynamic performance under different wave and wind conditions and more importantly to explore whether focused wave can replicate the features of irregular wave in the study of FOWT, a systematic study of NREL 5MW FOWT under a series of the incident wave and inflow wind is provided in this paper.

Totally, nine cases are simulated as summarized in Table 2 and Figure 3. LC1 and LC2 refer to the rated working conditions. The inflow wind speed is fixed as 10 m/s, slightly lower than the rated wind speed (11.4 m/s), but it is widely accepted in the study of NREL 5MW wind

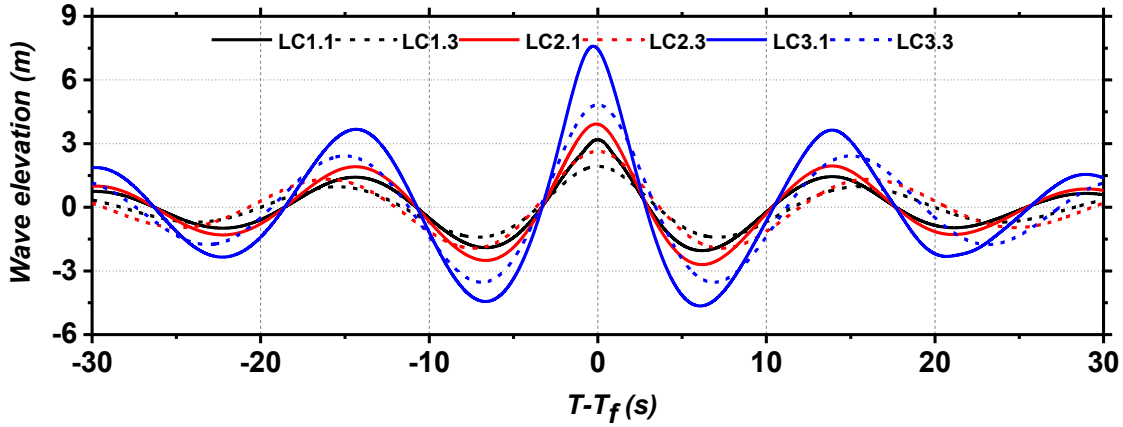

Figure 3 Wave elevation of LCs with focused wave types

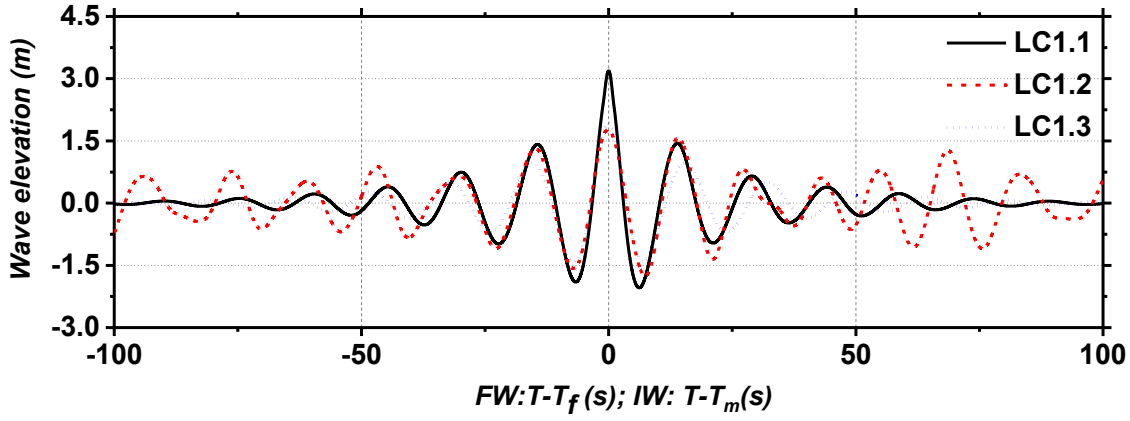

Figure 4 Wave elevation of LC1.1, LC1.2 and LC1.3

Table 2 Physical properties of the selected cases

Case No.		Wave type	Ao (m)	Hs(m)	Tp (s)	Hmax(m)	Thmax(s)	Wind
LC1	LC1.1	Focused	3.00	N/A	15.00	5.22	12.89	10m/s
	LC1.2	Irregular	N/A	1.94	15.00	3.32	14.45	
	LC1.3	Focused	1.91	N/A	16.20	3.33	13.94	
LC2	LC2.1	Focused	4.00	N/A	15.00	7.12	12.87	10m/s
	LC2.2	Irregular	N/A	2.49	15.00	4.62	15.08	
	LC2.3	Focused	2.64	N/A	16.80	4.62	15.15	
LC3	LC3.1	Focused	7.35	N/A	15.00	12.02	12.86	40m/s
	LC3.2	Irregular	N/A	5.13	15.00	8.33	14.01	
	LC3.3	Focused	4.83	N/A	15.70	8.37	13.74	

turbine. The blade pitch angle is maintained as a constant of 0° and the rotor speed is fixed as 12.1RPM for LC1 and LC2. LC3 represents extreme wind conditions, where the wind speed is as large as 40 m/s and the windstorms may occur. The rotor shuts down at all LC3 conditions and the output of aerodynamic power is treated as zero. Given a constant wind speed, we vary the sea state with two wave types and different wave parameters. Particularly, they are focused wave and irregular wave, and three linear wave amplitude (Ao) and wave peak periods (Tp), as indicated as LC1.x, LC2.x and LC3.x. Take the LC1 series as an example, LC1.1 and LC1.2 are constructed with the identical linear wave amplitude and wave peak period based on the NewWave theory. It should be noted that, even though the wave energy is the same between two waves, however, the energy distribution along the wave attack is not the same. Also, reproduced via the NewWave theory, LC1.3 is built up based on the largest wave of LC1.2 after 1000s full-time stochastic wave simulation in a Numerical Wave Tank (NWT). To be specific, the maximum wave height of LC1.3 is set as the same as the largest wave of LC1.2,

it is approximated by $A_{oLC*.3} = \frac{H_{maxLC*.2} * A_{oLC*.1}}{H_{maxLC*.1}}$. Figure 4 plots the wave elevations of LC1.1, LC1.2 and LC1.3. All focused wave modelling is computed for 300 seconds with the desired focused time setting at 150s. The selection of the focused time (150s) is determined by the natural dynamic responses of FOWT under wind & wave conditions, i.e., the FOWT usually reaches a maximum and a minimum motion response at t=55s and 110s, respectively, caused by the incident wind and the mean drift force. However, the transient phase mitigates near t=150s and the time-mean position of the floater reaches nearly a constant. Given an irregular wave case, modelling continues until 810 seconds.

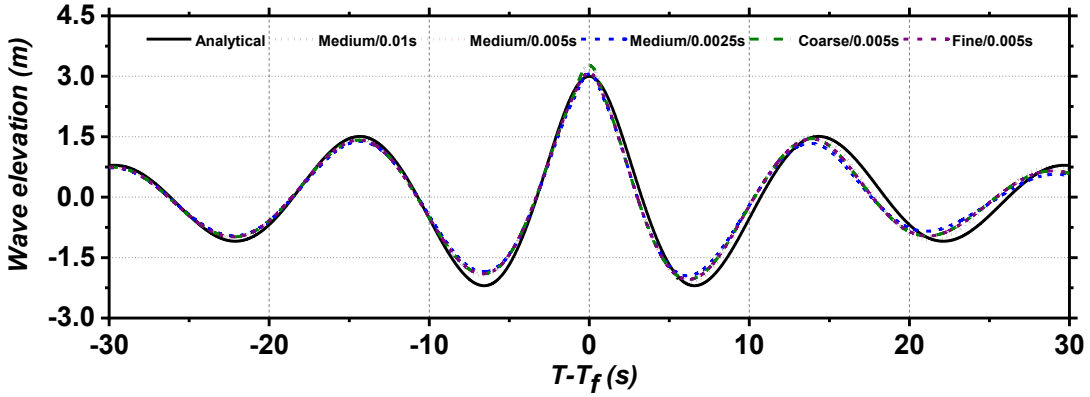

(a)

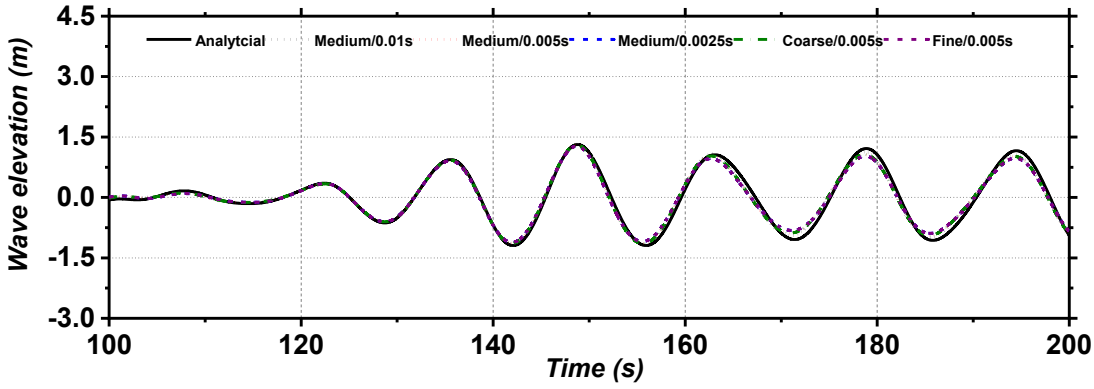

(b)

Figure 5 Mesh and time step convergence test of (a) focused wave and (b) irregular wave generation with Ao=6.0m Tp=15.0s

5. Results and Discussions

5.1 Validation and verification

In the present section, a 2D mesh and time step convergence test are carried out for the wave only generation. The numerical wave tank has the length of 750m (-250m<x<500m), the width of 2m (-1m<y<1m) and the height of 300m (-200m<z<100m). The water depth is set as 200m. The linear wave amplitude Ao of the NewWave refers to 3.0m and the wave peak period is Tp=15.0s, which are the parameters for LC1.1 and LC1.2 as summarised in Table 2. The focused position is set at $X_f = 0m$, and the focused time is set at 150s.

Table 3. CFD mesh configuration of 3 mesh densities under in the NWT (Ao=3.0m Tp=15.0s)

Refinement	Coarse	Medium	Fine
X axis	Δx= λ /150	Δx= λ /150	Δx= λ /300
Z axis	Δz= Ao/6	Δz= Ao/9	Δz= Ao/12
Slenderness Ratio	4.73	7.10	4.73

Three sets of mesh with different densities are generated; they are termed as Fine (38084), Medium (26668) and Coarse (20532), detailed in Table 3. Similarly, three time steps (Δt = 0.01s, 0.005s, and 0.0025s) are picked up for this sensitivity study. Figure 5 summarises the time history of wave amplitude with different mesh densities and time steps. It is seen that with sufficiently high mesh density and small time step, the results of predicted wave elevation are not sensitive to numerical parameters. Thus, the configuration of medium mesh is utilized in the following modelling to save the computational cost. Apart from the above numerical wave generation sensitivity study, the wave and FOWT structure interaction has been reported in our previous publication [23].

The present CFD solver has been validated via a series of benchmark FOWT cases in our previous studies [18, 23]. In detail, the coupled hydro-aero-mooring multiphase solver is carefully inspected by predicting the hydrodynamic responses of the semi-submersible floater, the aerodynamic loads of the wind turbine, and the tension loads of the mooring line for an

NREL 5MW wind turbine under the regular wave and uniform wind conditions. The results are aligned closely with the physical wave tank test of a 1/50 scaled model and the widely used NREL FAST tool based on a potential flow method and blade element method (BEM).

In addition, the focused wave studies have been examined in our previous papers, which started with the generation of a focused wave group in our numerical wave tank based on the deep-water first-order irregular wave theory. Moreover, due to the limited available data for a FOWT system under focused/extreme waves, we validated our CFD numerical model by investigating the wave-structure interaction of floating production storage and offloading (FPSO) subject to focused wave with available testing data in [14].

5.2 FOWT Hydrodynamics

5.2.1 Wave type influence (difference between Irregular wave and Focused wave)

Figure 6 (a) and (b) show the time history of the FOWT surge motions under LC1.*. In order to make the results clear and comparable, as shown in Figure 6 (c), the x-axis is normalised with the focused wave and irregular wave, where Tf =150s and Tm equals to the time at which

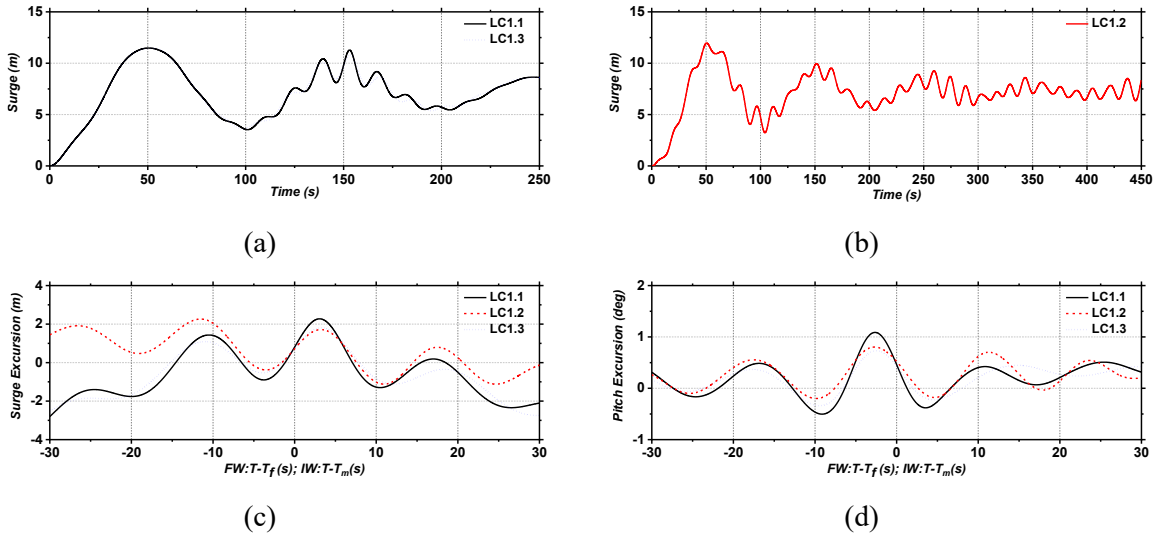

Figure 6 Dynamic motions of FOWT under LC1.1, LC1.2, and LC1.3 (a)(b) Surge (c) Surge Excursion (d) Pitch Excursion

the maximum wave crest is reached in the wave only simulation. The wind field modelling is activated at t=0s. The y-axis is normalised by the surge excursions which represents the FOWT offset surge motions regarding the time-mean surge motion. Similarly, the Figure 6 (d) shows the time history of the pitch excursions for LC1.*. As it is seen that, the disparities between the focused wave (LC1.1) and irregular wave (LC1.2) are notable when the FOWT experiences the surge peaks at T-T_f or T-T_m = 3.0s. The results of pitch motion for LC1.1 and LC1.2, as shown in Figure 6 (b), reveal that the pitch motion decreases significantly as the wave changes from a transient focused wave to a stochastic irregular wave. The variance of the FOWT dynamic motions subject to the irregular wave and the reconstructed focused wave is negligible from the results of LC1.2 and LC1.3 near the focused time. In particular, the surge and pitch motions match very well near the focused time, such as the well-captured troughs. Even though the absolute difference for the prediction of surge and pitch peak values is about 9.01% and 8.15%, respectively. Herein, the reconstructed focused wave shows its great potential to replicate a long time stochastic irregular wave on predicting the peak values.

In order to investigate the platform dynamic responses both in time and frequency domains, wavelet analysis is adopted in the current study as seen from Lin and Liu [35]. As suggested, the commonly used Fast Fourier Transform (FFT) is not perfectly applicable to transient sequence, such as the transient focused wave phenomenon observed herein. However, a continuous wavelet transform can predict both time and frequency characteristics simultaneously. In the present study, the Morlet wavelet method is chosen as the window function of wavelet transform, which is described as,

$$\psi_0(\mathrm{t}) = \pi^{-1/4}\mathrm{e}^{-t^2/2}\mathrm{e}^{-i\omega_0 t} \tag{16}$$

$$WT\,(s,\tau) = \int_{-\infty}^{+\infty} \eta(t)\psi^*_{s,\tau}\left(\frac{t-\tau}{s}\right)\mathrm{dt} \tag{17}$$

Where the ω_0 is the angular frequency of the wavelet. Furthermore, the continuous wavelet transform of a discrete wave train is defined as the convolution of a scaled and translated

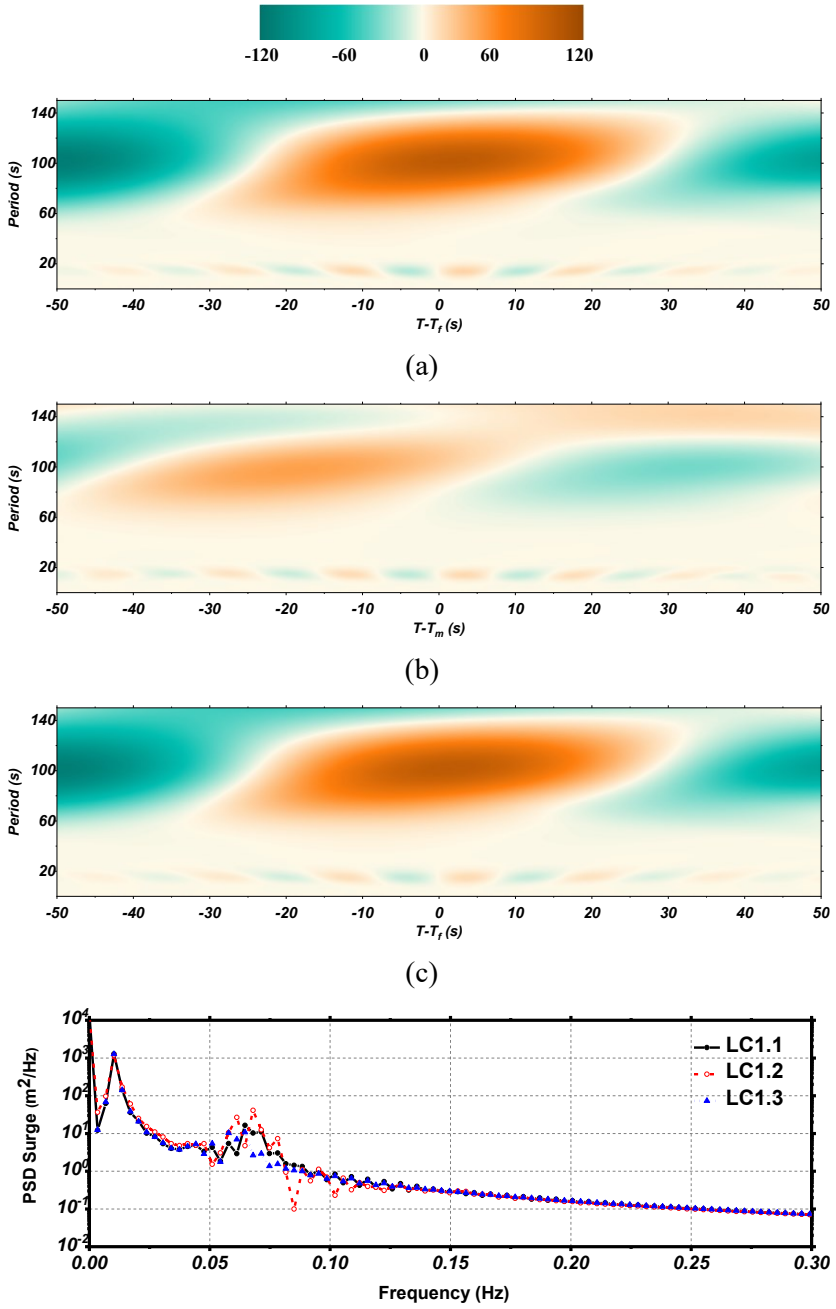

Figure 7 Wavelet analysis of surge motions under (a)LC1.1 (b)LC1.2 (c)LC1.3 and (d)PSDs of LC1

version of $\psi_0(\mathrm{t})$. Where the asterisk means the complex conjugate and the s is the wavelet scale.

As can be seen in Figure 7 (a) & (c), where the wavelet plots of surge motion under focused wave cases (LC1.1, and LC1.3) in time sequence are displayed, the wavelet energy bounces up significantly near the focused time for both cases. In addition, the period agrees commendably

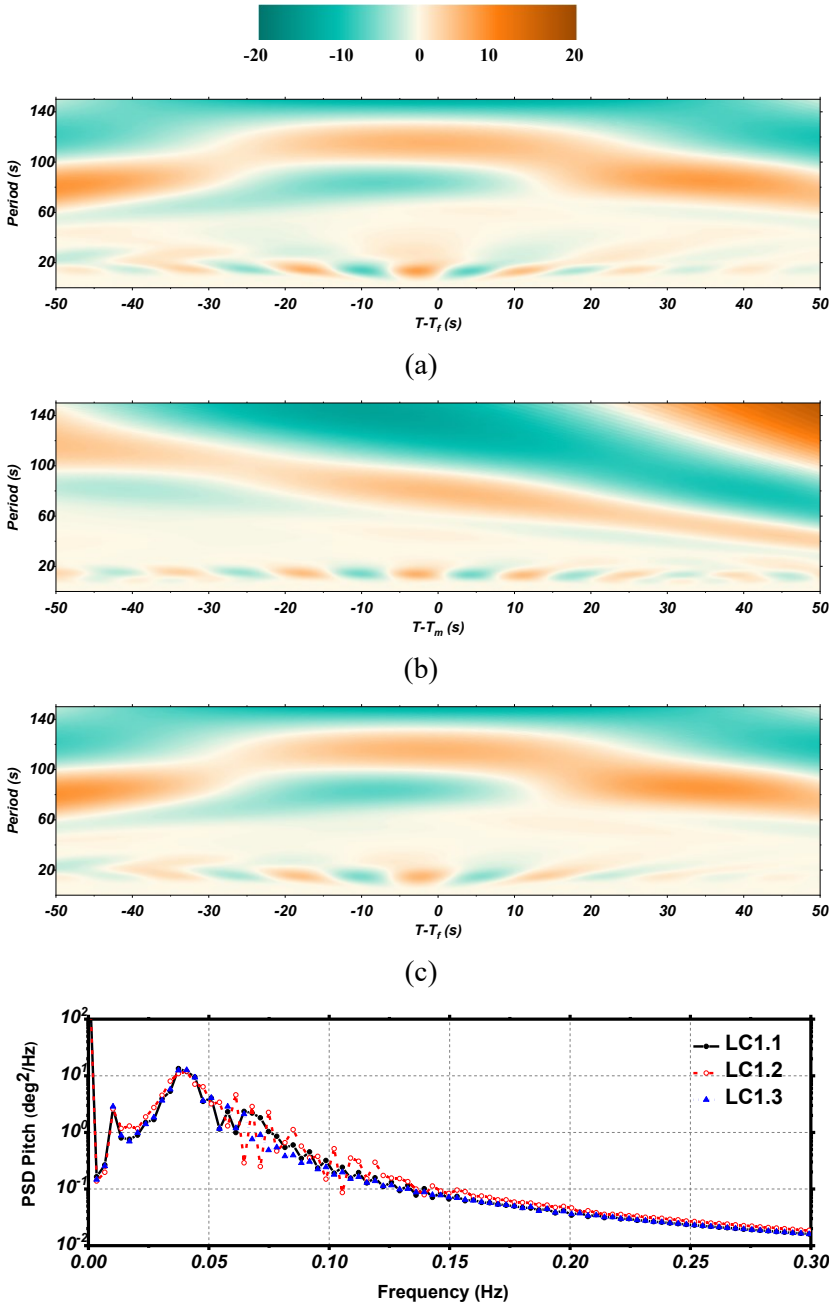

Figure 8 Wavelet analysis of pitch motions under (a)LC1.1 (b)LC1.2 (c)LC1.3 and (d)PSDs of LC1

with the incident wave period, i.e., Tp = 15.0s and Tp = 16.2s. Moving to the low frequency loads displayed at the top of each figure, it is noted that the energy bumps up near the floater's

surge natural period and quickly spreads over the entire time series. This might be due to the free decay motion together with the second-order difference frequency loads, and the transient focused wave may also induce a sudden load to the floater, which excites the resonance. The wavelet plots under long-term stochastic irregular wave are provided in Figure 7 (b), similar to the plots in Figure 7 (a) & (c) associated with focused wave, here, we obtained both the wave energy and the low frequency loads under irregular wave. Differently, the energy close to the incident wave frequency, exits in the overall time domain. To have a better understanding of how wavelet analysis acts differently from FFT analysis, the PSDs of surge motion of LC1 is given in Figure 7 (d). It is seen that the peak near f = 0.7Hz is well captured, indicating the incident wave energy range of three cases. Besides, a very low frequency peak at f = 0.01Hz is observable, which coincides to the natural surge frequency. Figure 8 (a)-(c) display the relevant pitching motion wavelet transforms. Generally, the results are like those for surge motion indicated in Figure 7. However, another low frequency energy appears around 20-40 seconds close to pitch natural frequency. Nevertheless, the occurrence of a high-frequency load is found in Figure 8 (b) at T-Tm=30s for an irregular wave study. The PSDs of pitch motion is plotted in Figure 8 (d), the peaks are seen for all three cases simultaneously at f = 0.037 Hz.

Table 4 Statistics of excursion values of wind turbine motions under different LCs

		U=10.0 m/s, Turbine operating						**U=40.0m/s, Turbine shut**		
		LC1.1	LC1.2	LC1.3	LC2.1	LC2.2	LC2.3	LC3.1	LC3.2	LC3.3
Surge	Max (m)	2.27	1.81	1.71	2.72	2.06	2.11	4.36	3.24	3.22
	Min (m)	-0.90	-0.52	-0.41	-1.45	-0.61	-1.03	-2.69	-2.16	-2.60
Heave	Max (m)	0.80	0.88	0.67	1.12	0.91	0.87	2.36	1.80	1.99
	Min (m)	-0.86	-0.94	-0.66	-1.13	-0.93	-0.83	-2.18	-2.01	-1.99
Pitch	Max (deg)	1.08	0.80	0.73	1.47	0.91	1.11	3.61	1.79	2.13
	Min (deg)	-0.50	-0.19	-0.33	-0.74	-0.42	-0.57	-1.48	-0.92	-1.18

Furthermore, we carry out a statistical analysis based on the maximum excursion of the floater motion data summarised in Table 4. Generally, it is revealed that, given the similar linear crest height (LC1, LC2, and LC3), the motion predictions are similar. However, whether it is an irregular wave or a focused wave has a large impact on the motion. Using the identical linear wave amplitude and wave peak period in NewWave theory under LCx.1 and LCx.2, for instance, the focused wave induces reasonably higher peaks than irregular wave due to a relatively higher wave elevation under identical motion response amplitude operator (RAO). In addition, a comparison between LCx.2 and reconstructed focused wave LCx.3 indicates that reconstructed focused waves can capture much closer motion response due to be the aligned incident maximum wave loads within a much cheaper computational cost.

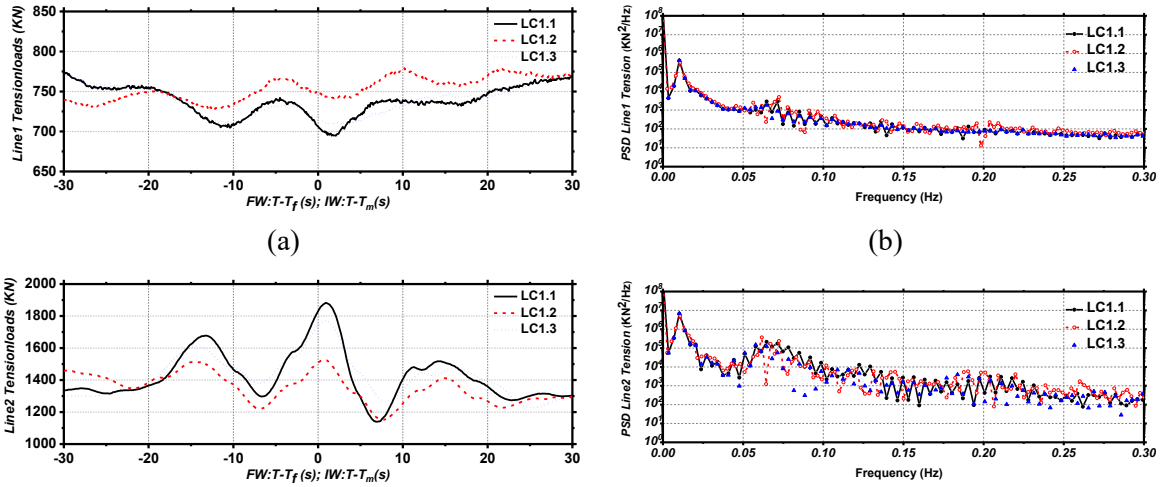

Figure 9 Tension loads of Line1 and Line2 and PSDs analysis for a FOWT subject to LC1.1, LC1.2 and LC1.3 (a) Tension loads of mooring line1 (b) PSDs of tension loads of mooring line1 (c) Tension loads of mooring line2 (d) PSDs of tension loads of mooring Line1

The time sequence of tension loads as well as the PSDs of mooring lines are shown in Figure 9. In the time domain, the variation of mooring tensions is similar to the surge motion predictions of FOWT shown in Figure 6. This is reasonable as the tension load is another determinant parameter to constrain the platform motion. We can witness the variance among LC1.1-1.3 due to different offset position of the floater under a focused wave and an irregular

wave condition. From the spectral analysis shown in Figure 9 (b) & (d), there are a few peak frequencies. The first one occurs at f = 0.01Hz corresponding to the natural surge frequency, mainly induced by the nonlinear loads. Other high frequency peaks are within the wave energy range, representing the linear results.

5.2.2 Wave steepness influence

This section describes the FOWT dynamic responses under different wave steepness. For the ease of discussion, only LC*.1 and LC*.2 are included in this section. It is worthwhile to mention that the wind speed for LC1 and LC2 is 10.0 m/s while that for LC3 40 m/s.

Figure 10 (a) & (c) plots the surge and pitch motions near the focused time for the above three cases. It is shown that the FOWT experiences a dramatic motion response near the focused time under LC3.1. In fact, the maximum surge and pitch motion increase almost 3.88 meters and 3.51 degrees compared with the LC1.1. The power spectral analysis of the surge and pitch

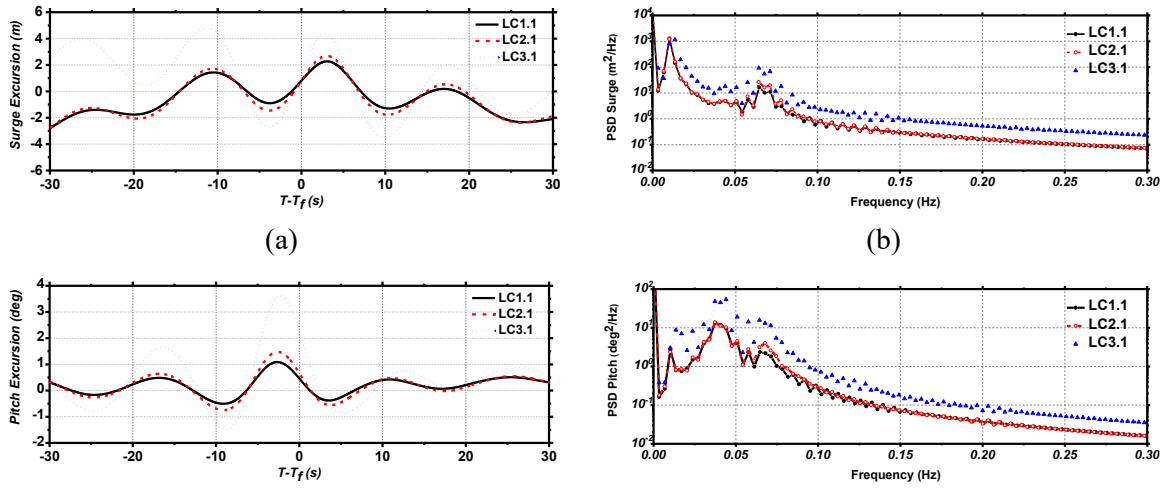

Figure 10 FOWT surge and pitch motions and PSDs under LC1.1, LC2.1 and LC3.1 (a)Surge (b) Surge PSDs (c)Pitch (d)Pitch PSDs

responses is illustrated in Figure 10 (b) & (d), where several important peaks are well captured. Specifically, the peak near 0.67Hz accurately captures the surge response in the wave energy

range for LC*.1. Since the natural pitch frequency of the FOWT is at *f=0.037Hz*, in the pitch PSDs, the peak near natural pitch frequency is found alongside with the peak at *f=0.01Hz*. It is obvious that the increase of the wave height leads to the increase of nonlinear peaks as a result of wave nonlinearity growing. This finding is consistent with our previous studies [18].

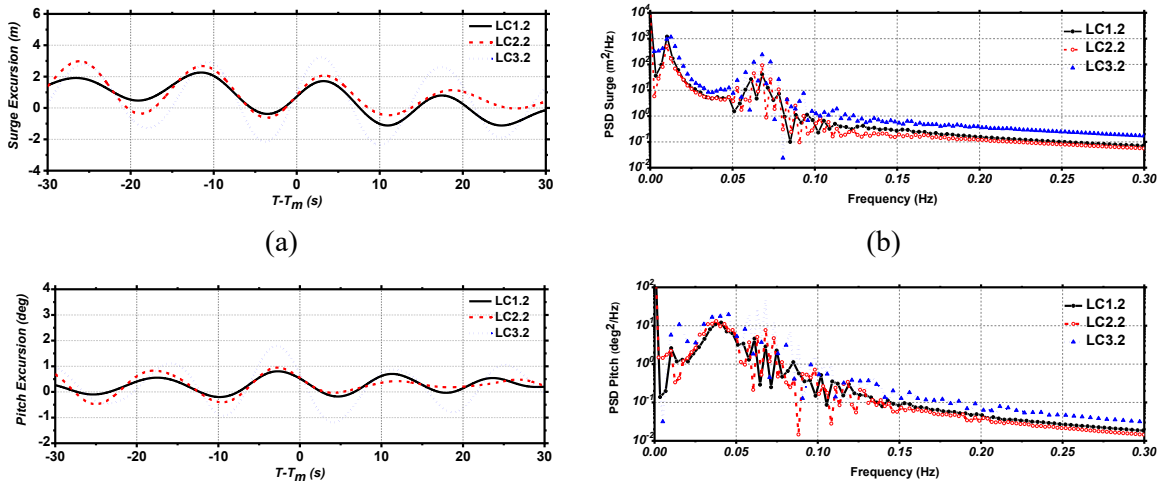

Figure 11 FOWT surge and pitch motions and PSDs under LC1.2, LC2.2 and LC3.2 (a)Surge (b)Surge PSDs (c)Pitch (d)Pitch PSDs

Figure 11 (a)-(d) plot the surge and pitch motions together with PSD of the irregular wave cases under different wave steepness. Generally, the dynamic motions and the motion PSDs behave simillarlly with the results revealed under LC*.1. Interestingly, if we focus on the low frequency range for pitch PSDs shown Figure 11 (d) when $f < fp=0.067Hz$, *under* LC3.2, a significant rise in the nonlinear peaks near surge and pitch natural frequency could be witnessed compared with LC1.2 and LC2.2.

The surface elevation contour plots are presented in Figure 12 for LC1.1. It is seen that the nonlinear wave-structure interaction, such as the wave diffraction and radiation are well captured by using our numerical modelling. Moreover, those wave-structure interactions become more significant around the focused time, as indicated by the relatively high wave run-up near semi-submersible floater. The relevant plots for LC3.1 for extreme sea state, displayed in Figure 13, reveal much higher wave-run ups around upstream and starboard

columns at the focused time. Moreover, a stronger wave diffraction and radiation is evident around the side columns, which is hardly observed given a normal sea state.

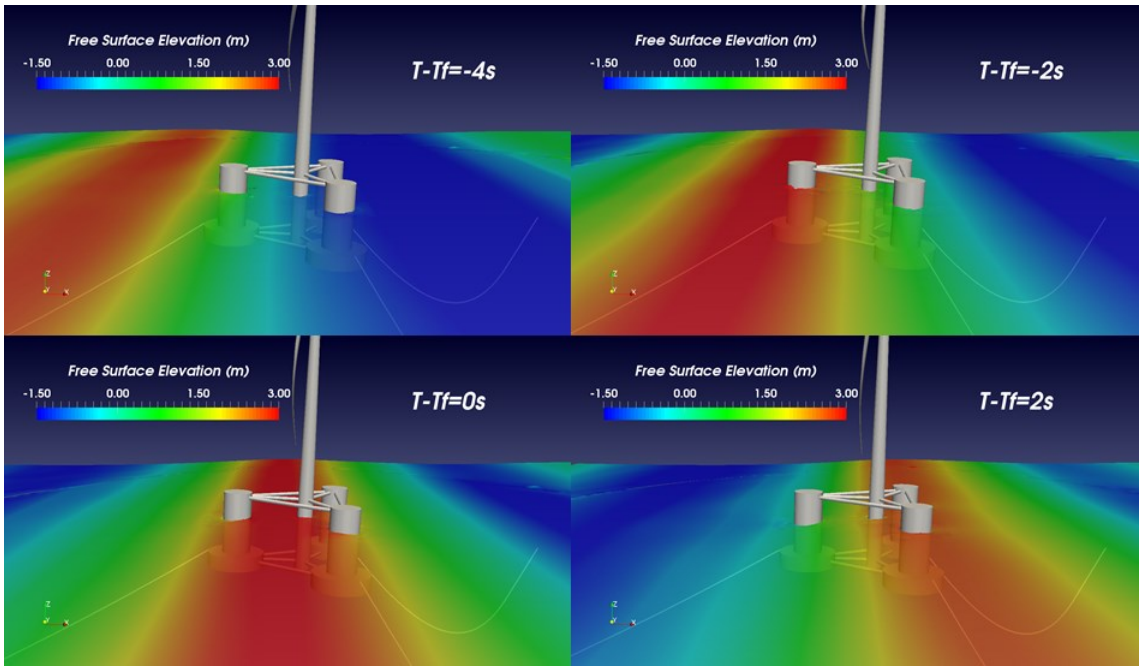

Figure 12 Wave elevation contour plots of LC1.1

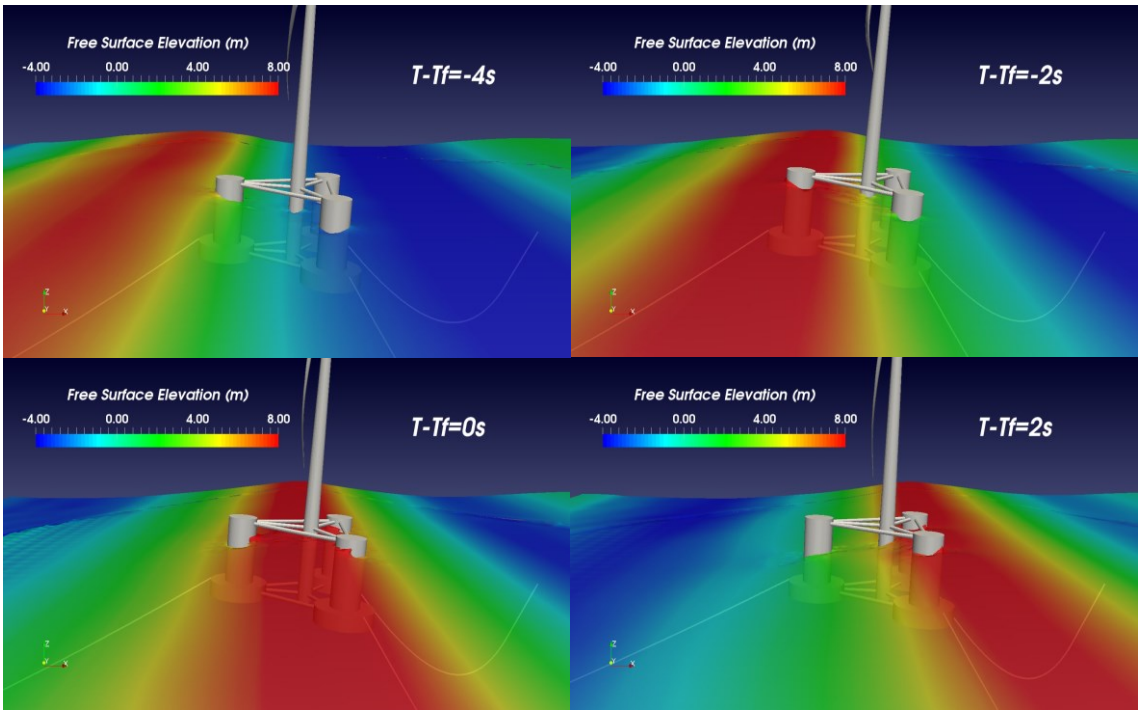

Figure 13 Wave elevation contour plots of LC3.1

5.3 FOWT aerodynamics

This section discusses the FOWT aerodynamic characteristics with the change of wave types and sea state. Figure 14 plots the thrust force and the power output of the turbine in time sequence for different LCs excluding LC3. As seen, the thrust and power follow a similar pattern as the response of pitch motion of FOWT shown in Figure 6. This provides strong evidence that, among six degrees of freedom floating platform motions, the pitch motion has the most significant impact on wind turbine aerodynamics via modulating the swept area of the turbine.

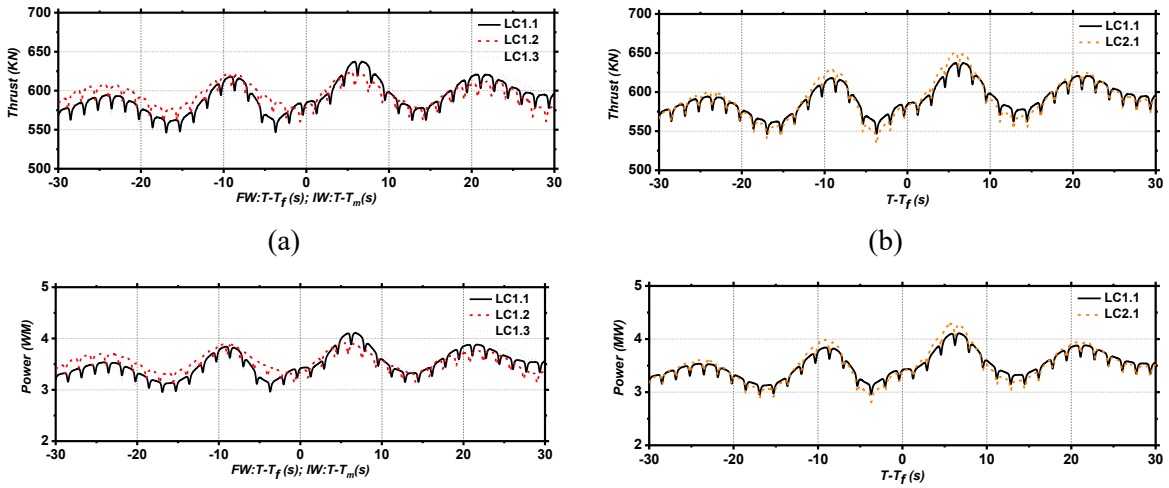

Figure 14 Thrust outputs of FOWT (a) LC1 (b) LC1.1 &LC 2.1; power outputs of FOWT under (a) LC1 (b) LC1.1 &LC2.1

Specifically, regarding the wave type impacts indicated from Figure 14 (a) & (c), we can see that the local minimum values are captured simultaneously due to the existence of tower shadow effect. Interestingly, the discrepancy among three cases is not as significant as the difference in pitch motion. In addition, Figure 14 (b) & (d) also indicate that the peaks near T-Tf = -2s are the same for both cases. One of the possible explanations is due to the small difference associated with the swept area for both cases. Therefore, we can conclude that, the incident wave has less impact on turbine aerodynamic characteristics than its influence on

motion responses of floater, which shows the nice floater stability and small wave induced motions in the power productions.

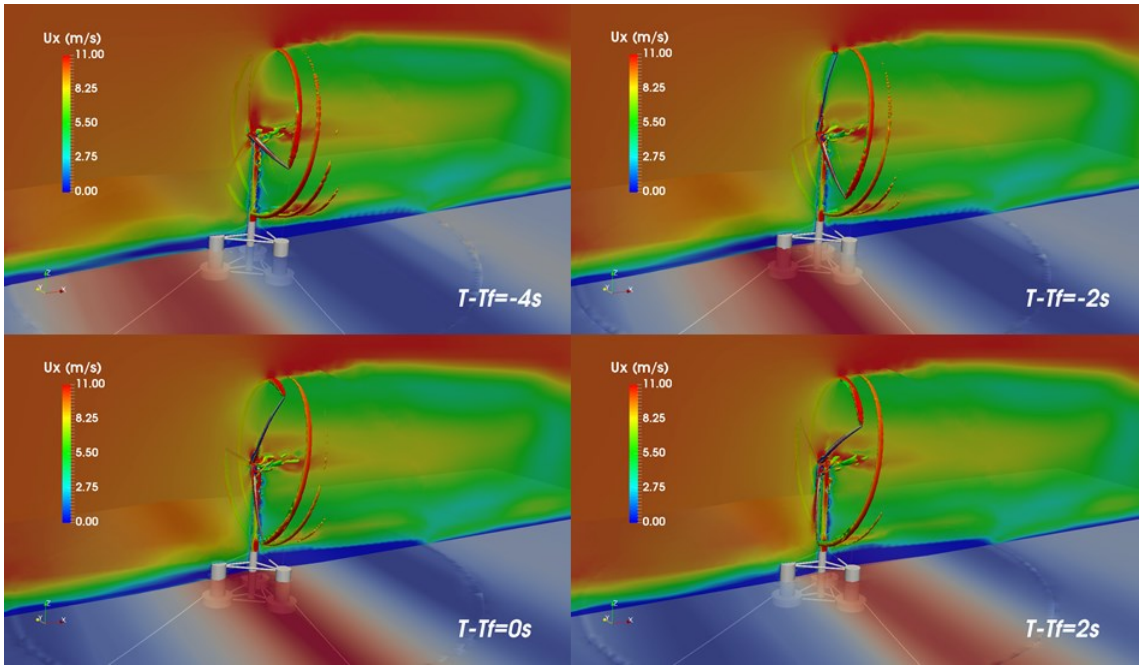

Figure 15 Instantaneous flow field on the sectional vertical mid-plane (XoZ) colored by axial velocity under LC1.1

Figure 15 shows the instantaneous velocity contour on the XoZ plane at Y=0m together with the wave propagation at different instantaneous time near the focused time for LC1.1. The vortex contour of the second invariant of the rate of strain tensor Q [36] coloured by velocity component Ux is plotted at the turbine wake, i.e., Q refers to 1. Figure 15 shows the existence of wave-wind interaction coupled in the CFD modelling evidenced by a low-speed flow regime close to the free surface, leading to focused wave crests attributed to the decreased axial velocity. On the aerodynamics side, the turbine wake is well resolved.

As a key parameter to evaluate a floating wind turbine's structural damage, the tower bending moment, calculated by y component of the cross product of the distance vector and the turbine aerodynamic force vector, is analysed and investigated. Since the entire FOWT is treated as a rigid system, hence, the structural response of the tower is determined by the global motion

response of the FOWT. The time history of tower-base bending moment and PSDs of LC1.x and LCx.1 are shown in Figure 16. It can be seen that the incident wave energy range is in agreement with the wave peak frequency at f=0.67Hz. Moreover, two peaks are observed at second-order difference frequency wave loads, i.e., at f=0.01Hz for FOWT surge and f = 0.037Hz for FOWT pitch natural frequency, respectively.

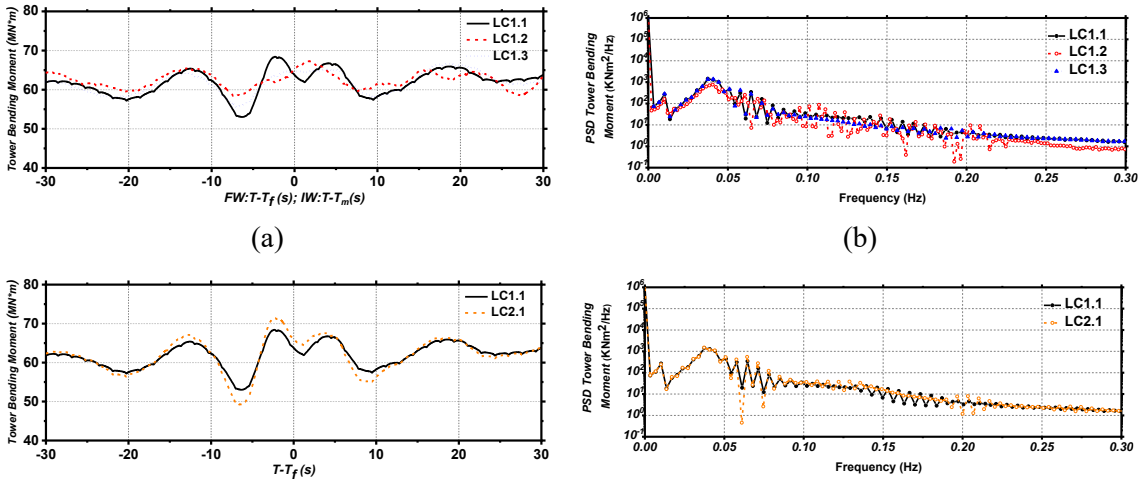

Figure 16 Tower base bending moment under (a)LC1 (c)LC1.1&LC2.1; PSDs of tower base bending moment under (b)LC1 (d)LC1.1&LC2.1

6. Conclusion

The current study presents an investigation into a semi-submersible NREL 5MW floating offshore wind turbine and its hydro/aero-dynamics predictions under various wave types and wave steepness. The modelling was achieved by using a high-fidelity CFD tool considering the fully nonlinear wave-wind-structure interaction.

Generally, an observable variance presents under both surge and pitch motions between LCx.1 and LCx.2. The comparison between LCx.2 and LCx.3 reveals that the reconstructed focused wave shows its great potential for replicating the maximum/minimum dynamic motion excursions predicted by irregular wave. This is because we applied the same maximum wave loads for LCx.2 and LCx.3. Different sea state studies show that an increase of the wave

steepness will lead to the nonlinear load arising at FOWT structure natural frequencies, this is consistent with the results found in our previous study [18].

For the turbine aerodynamics, the thrust and power output reach several peaks near focused time caused by the platform motion, and the pitch motion is believed to be a prominent factor to affect turbine aerodynamics other than wind speed and wind direction due to the change of the swept area. The results also indicate that the variation of incident wave has less impact on aerodynamics of the turbine than the dynamic motion of the floater.

With the above conclusions, some recommendations of the applicability of focused wave can be given as follows: adopting the same linear wave amplitude and wave peak period in NewWave theory with two different wave types, i.e., LCx.1 & LCx.2, focused wave overestimates the dynamic response and the mooring line tension loads than irregular wave. Nevertheless, this variance becomes closer while adopting reconstructed focused wave LCx.3. Taking all factors into consideration, such as the computational costs, the predictions of hydrodynamic/aerodynamic loads and the wave reflection, utilizing a focused wave is more rigorous and appropriate than using an irregular wave to study the offshore floating structures including FOWT.

Acknowledgement

This work used the Cirrus UK National Tier-2 HPC Service at EPCC (http://www.cirrus.ac.uk) funded by the University of Edinburgh and EPSRC (EP/P020267/1) and ARCHIE-WeSt High Performance Computer (www.archie-west.ac.uk) based at the University of Strathclyde. Yang Zhou thanks China Scholarship Council (CSC) for financial support during his study in the UK.

Reference

[1] Ramírez, L., Fraile, D., and Brindley, G., 2021, "Offshore wind in Europe: Key trends and statistics 2020."

[2] Dysthe, K., Krogstad, H. E., and Müller, P., 2008, "Oceanic rogue waves," Annu. Rev. Fluid Mech., 40, pp. 287-310.

[3] Davis, M., 1964, "Testing ship models in transient waves," the 5th Symposium on Naval Hydrodynamics, ONR, Bergen, Norway, pp. 507-544.

[4] Baldock, T., Swan, C., and Taylor, P., 1996, "A laboratory study of nonlinear surface waves on water," Philosophical Transactions of the Royal Society of London. Series A: Mathematical, Physical and Engineering Sciences, 354(1707), pp. 649-676.

[5] Ryu, Y., Chang, K.-A., and Mercier, R., 2007, "Application of dam-break flow to green water prediction," Applied Ocean Research, 29(3), pp. 128-136.

[6] Orszaghova, J., Taylor, P. H., Borthwick, A. G., and Raby, A. C., 2014, "Importance of second-order wave generation for focused wave group run-up and overtopping," Coastal Engineering, 94, pp. 63-79.

[7] Liang, X. F., Yang, J. M., Li, J., Xiao, L. F., & Li, X. , 2010, "Numerical simulation of irregular wave-simulating irregular wave train," Journal of Hydrodynamics, 22(4), pp. 537-545.

[8] Niu, X., Ma, X., Ma, Y., and Dong, G., 2020, "Controlled extreme wave generation using an improved focusing method," Applied Ocean Research, 95, p. 102017.

[9] Xu, L., Barltrop, N., and Okan, B., 2008, "Bow impact loading on FPSOs 1—experimental investigation," Ocean Engineering, 35(11-12), pp. 1148-1157.

[10] Draycott, S., Steynor, J., Davey, T., and Ingram, D. M., 2018, "Isolating incident and reflected wave spectra in the presence of current," Coastal Engineering Journal, 60(1), pp. 39-50.

[11] Fang, Z., Xiao, L., Wei, H., Liu, M., and Guo, Y., 2020, "Severe wave run-ups on fixed surface-piercing square column under focused waves," Physics of Fluids, 32(6), p. 063308.

[12] Gao, N., Yang, J., Tian, X., and Li, X., 2016, "A numerical study on the nonlinear effects in focused wave modelling and forces on a semi-submerged horizontal cylinder," Ships and Offshore Structures, 12(4), pp. 474-485.

[13] Westphalen, J., Greaves, D., Williams, C., Hunt-Raby, A., and Zang, J., 2012, "Focused waves and wave–structure interaction in a numerical wave tank," Ocean Engineering, 45, pp. 9-21.

[14] Mai, T., Greaves, D., Raby, A., and Taylor, P. H., 2016, "Physical modelling of wave scattering around fixed FPSO-shaped bodies," Applied Ocean Research, 61, pp. 115-129.

[15] Ransley, E., Yan, S., Brown, S. A., Mai, T., Graham, D., Ma, Q., Musiedlak, P.-H., Engsig-Karup, A. P., Eskilsson, C., and Li, Q., 2019, "A blind comparative study of focused

wave interactions with a fixed FPSO-like structure (CCP-WSI Blind Test Series 1)," International Journal of Offshore and Polar Engineering, 29(02), pp. 113-127.

[16] Brown, S. A., Musiedlak, P.-H., Ransley, E. J., and Greaves, D., 2018, "Numerical simulation of focused wave interactions with a fixed FPSO using OpenFOAM 4.1," The 28th International Ocean and Polar Engineering Conference, International Society of Offshore and Polar Engineers.

[17] Draycott, S., Nambiar, A., Sellar, B., Davey, T., and Venugopal, V., 2019, "Assessing extreme loads on a tidal turbine using focused wave groups in energetic currents," Renewable Energy, 135, pp. 1013-1024.

[18] Zhou, Y., Xiao, Q., Liu, Y., Incecik, A., Peyrard, C., Li, S., and Pan, G., 2019, "Numerical modelling of dynamic responses of a floating offshore wind turbine subject to focused waves," Energies, 12(18), p. 3482.

[19] Bredmose, H., and Jacobsen, N. G., 2010, "Breaking wave impacts on offshore wind turbine foundations: focused wave groups and CFD," International Conference on Offshore Mechanics and Arctic Engineering, pp. 397-404.

[20] Ransley, E., Greaves, D., Raby, A., Simmonds, D., and Hann, M., 2017, "Survivability of wave energy converters using CFD," Renewable Energy, 109, pp. 235-247.

[21] Zhao, X., and Hu, C., 2012, "Numerical and experimental study on a 2-D floating body under extreme wave conditions," Applied Ocean Research, 35, pp. 1-13.

[22] Van Der Meulen, M. B., Ashuri, T., Van Bussel, G. J., and Molenaar, D. P., 2012, "Influence of nonlinear irregular waves on the fatigue loads of an offshore wind turbine," The Science of Making Torque from Wind; 4th scientific conference, Oldenburg, 9-12 Oct, 2012, Citeseer.

[23] Liu, Y., Xiao, Q., Incecik, A., Peyrard, C., and Wan, D., 2017, "Establishing a fully coupled CFD analysis tool for floating offshore wind turbines," Renewable Energy, 112, pp. 280-301.

[24] Liu, Y., Xiao, Q., Incecik, A., and Peyrard, C., 2019, "Aeroelastic analysis of a floating offshore wind turbine in platform-induced surge motion using a fully coupled CFD-MBD method," Wind Energy, 22(1), pp. 1-20.

[25] Jonkman, J., Butterfield, S., Musial, W., and Scott, G., 2009, "Definition of a 5-MW reference wind turbine for offshore system development," National Renewable Energy Lab.(NREL), Golden, CO (United States).

[26] OpenFOAM, 2019, "The OpenFOAM Foundation Website."

[27] Hirt, C. W., and Nichols, B. D., 1981, "Volume of fluid (VOF) method for the dynamics of free boundaries," Journal of computational physics, 39(1), pp. 201-225.

[28] Jacobsen, N. G., Fuhrman, D. R., and Fredsøe, J., 2012, "A wave generation toolbox for the open-source CFD library: OpenFoam®," International Journal for numerical methods in fluids, 70(9), pp. 1073-1088.

[29] Lindgren, G., 1970, "Some properties of a normal process near a local maximum," Annals of Mathematical Statistics, 41(6), pp. 1870-1883.

[30] Boccotti, P., 1983, "Some new results on statistical properties of wind waves," Applied Ocean Research, 5(3), pp. 134-140.

[31] Jacobsen, N. G., van Gent, M. R., and Wolters, G., 2015, "Numerical analysis of the interaction of irregular waves with two dimensional permeable coastal structures," Coastal Engineering, 102, pp. 13-29.

[32] Hu, Z. Z., Greaves, D., and Raby, A., 2016, "Numerical wave tank study of extreme waves and wave-structure interaction using OpenFoam®," Ocean Engineering, 126, pp. 329-342.

[33] Liu, Y., 2018, "A CFD study of fluid-structure interaction problems for floating offshore wind turbines," PhD thesis, University of Strathclyde.

[34] Morison, J., Johnson, J., and Schaaf, S., 1950, "The force exerted by surface waves on piles," Journal of Petroleum Technology, 2(05), pp. 149-154.

[35] Lin, E.-B., and Liu, P. C., 2004, "A discrete wavelet analysis of freak waves in the ocean," Journal of Applied Mathematics, 2004(5), pp. 379-394.

[36] Li, Y., Paik, K.-J., Xing, T., and Carrica, P. M., 2012, "Dynamic overset CFD simulations of wind turbine aerodynamics," Renewable Energy, 37(1), pp. 285-298.